
Tool and process development for chambering bores with non-circular contour in highly stressed workpieces

Julian Frederic Gerken, Robert Schmidt
and Dirk Biermann

Institute of Machining Technology,
TU Dortmund University,
Baroper Str. 303, 44227, Dortmund, Germany
Email: julian.gerken@tu-dortmund.de
Email: robert2.schmidt@tu-dortmund.de
Email: biermann@isf.de
*Corresponding author

Moritz Fuß

BGTB GmbH,
Dorstfelder Hellweg 60,
44149 Dortmund, Germany
Email: m.fuss@bgtd.de

Abstract: A novel chamber boring system allows for contouring of boreholes in axial and radial direction to produce special profiles required from oil industry. The machined contour, produced by this system, consists of six convexities in radial direction. In this paper, the development of the cutting tool and its kinematics are described. Due to the fully mechanical drive of the system, different tool designs cause a distortion of the resulting contour. In addition, the cutting parameters also affect the machined profile. The resulting contour deviations were analysed and measured by a 3D-coordinate-measuring-system. To ensure transferability to industrial applications, a process strategy with re-cutting after a tool change was developed and analysed using an optical 3D measurement system. With this strategy and the improved tool kinematics, it is possible to machine a workpiece with a length of $l = 2500$ mm. Future research projects investigate the possibility to substitute the mechanical drive with an electrical drive.

Keywords: chamber boring system; deep hole drilling; strain gauge; torque measurement; tool development; process optimisation; internally profiled workpieces with small internal diameters; MUD drive production.

Reference to this paper should be made as follows: Gerken, J.F., Schmidt, R., Biermann, D. and Fuß, M. (2021) 'Tool and process development for chambering bores with non-circular contour in highly stressed workpieces', *Int. J. Mechatronics and Manufacturing Systems*, Vol. 14, Nos. 3/4, pp.289–304.

Biographical notes: Julian Frederic Gerken studied Mechanical Engineering at the TU Dortmund University. From 2017 to 2019, he worked as a Technical Project Engineer for automated recycling crane systems at Demag Cranes and

Components GmbH. Since July 2019, he works as a research associate in the Department of Machining Technology at the Institute of Machining Technology (ISF) at the TU Dortmund University. The main research activities deal with ejector and BTA-deep-hole drilling processes.

Robert Schmidt studied Mechanical Engineering at the TU Dortmund University. Since July 2017, he works as a Research Associate in the Department of Machining Technology, focusing on processes with geometric defined cutting edges, at the Institute of Machining Technology (ISF) at the TU Dortmund University. The main research activities deal with deep-hole drilling processes, especially the BTA deep-hole drilling process.

Dirk Biermann studied Mechanical Engineering at the University of Dortmund and received his doctorate in the field of Machining Technology. During his eight years in industry, he was responsible for the production of combustion engines as head of production at Dr. SCHRICK GmbH in Remscheid. Since April 2007, he has been head of the Institute of Machining Technology (ISF) at the TU Dortmund University. From 2011 to 2012, he was Dean of the Faculty of Mechanical Engineering and from 2014 to 2016 Vice Rector Research at the TU Dortmund University. In 2019 he was appointed Honorary Professor at the University of Nanjing of Aeronautics and Astronautics, China. Prof. Biermann is a Fellow of the International Academy for Production Engineering (CIRP) and a member of the Scientific Society for Production Engineering (WGP).

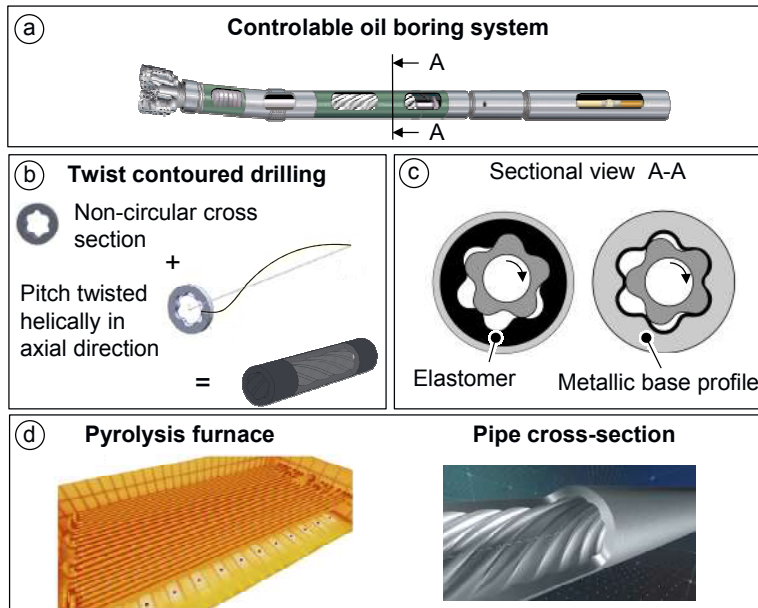
Moritz Fuß studied Mechanical Engineering at the TU Dortmund University. Since 2013, he worked as a Research Associate in the department of Machining Technology at the ISF until December 2019 and received his doctorate in the field of Machining Technology in August 2019. Since January 2020 he works for the Beratende Gesellschaft für Tiefbohr- und Zerspanungstechnik (BGTB GmbH). As a cooperation partner of the ISF at TU Dortmund University, he continuously carries out research projects and participates, together with the BGTB GmbH, in numerous research projects related to deep drilling.

1 Introduction

In some highly technical industrial areas components with deep bore holes with internal contours are increasingly being used. The aviation industry, the petrochemical industry and the petrol chemistry are three industries which make use of these contoured bores. For example, the huge advantage for the aviation industry is the weight reduction of landing gears for aircrafts compared to massive components (Biermann, 2018; Buse, 1994). The state of the art is to produce such rotationally symmetric inner contours by using chamber boring techniques. For special components used, for example, in the oil extraction and processing industry, rotationally symmetrical inner contours are not sufficient. Such components like motor stators in drill pipes or flow-conducting pipes for process engineering require non circular profiles. In the context of this scientific work, a new cutting process suitable for the production of these parts is presented, which extends the current chamber boring process by a further dimension. This is implemented by a tooling system in which the cutting edge moves radially out and in periodically per evolution depending on the profile contour to be produced (Biermann, 2018).

Tubes with non-circular profiles are used in the oil exploration as a stator in mud motors. Mud motors, are in principal positive displacement pumps or moineau pumps named after their creator ‘Moineau’. The mud motors are based on the inversion of this pump principle. Pressurised dill fluid is guided to the motor/pump to achieve a rotation of the shaft. These motors and techniques are mainly used in the directed drilling for the gas and oil exploration. A system for the directed drilling is shown in Figure 1(a).

Figure 1 Possible usage of the non-circular profile (see online version for colours)



Source: Fuß (2016) and Malcore (2010)

The motor consist of three main components: The rotor, the stator and an elastomer seal. While the non-circular cross section of the rotor (Figure 1(c)) is machineable in nearly all sizes, the inner profile of the stator (Figure 1(b)), especially for smaller diameters ($D < 75$ mm), remains a challenge (Baker Hughes, 2020). Instead of machining, an elastomer with the non-circular cross section is placed inside a metal tube (Figure 1(c), left). Stators with larger diameters can be machined with a metallic base profile and a thin elastomer layer, resulting in an efficiency enhancement up to 100% compared to elastomer profiles (Fuß et al., 2016; Maurer, 2000).

Up until now there is no process which can produce the required metallic base profile in smaller diameters economically with a standard machining processes. Due to this technological gap the advantage of a metallic base profile cannot be utilised in components with smaller bore diameters ($D < 75$ mm) (Denkena et al., 2016; Heisel, 1989). There are manufacturing processes such as tube drawing, which can produce such inner profiles but these processes are not suitable for small batch production and are also very time-consuming, cost-intensive and inflexible (Bottos and Underwood, 2003). The objective of this project is the result of the growing demand for small non circular inner profiles in long tubes. The novel AK-UR-drive (out-of-round chambers, translated from

German) was developed and later proven by machining stators made of aluminium and AISI 4140 in lengths of up to $l_f = 2600$ mm (Fuß et al., 2016).

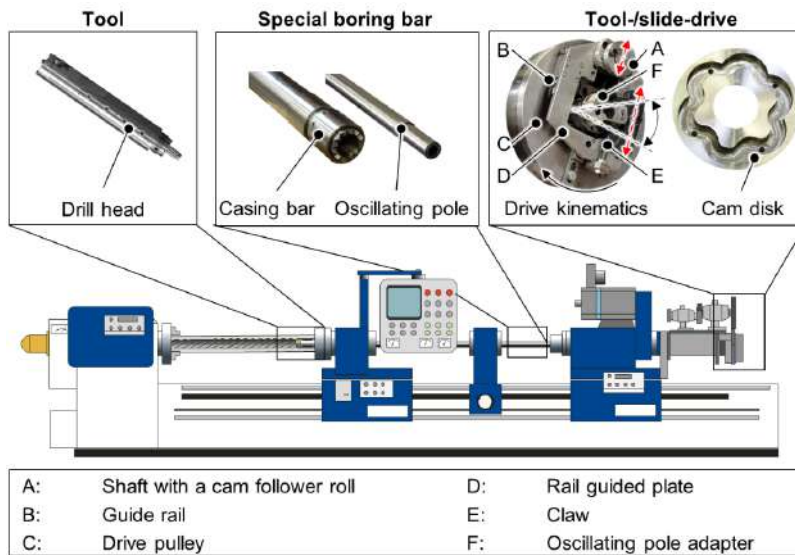
2 Methodology and research boundaries

The experimental investigations on the AK-UR-process (out-of-round chambers) were carried out on a horizontal BTA deep drilling machine of the type Giana GGB 560. The machine is operated by a Sinumerik 840D sl and contains the usual assemblies for it, control, workpiece headstock, tool headstock, guide carriage with mounted drilling oil supply apparatus (BOZA) and torsional damper, which are all mounted on the machine bed.

2.1 BTA deep drilling machine with AK-UR drive

To produce the internally profiled bores, a shaft with a suitable pilot bore is required to guide the drill head. The system is designed to be adapted to a BTA deep drilling machine to machine long workpieces, without affecting the original function of the machine. Figure 2 shows the adapted AK-UR drive and the BTA deep hole drilling machine schematically.

Figure 2 Chamber boring system adapted to the Giana GGB 560 (see online version for colours)



The casing bar ($l = 3900$ mm, $d = 39$ mm) extends through the tool headstock to the rear and is connected to the tool drive for radial movement by means of an adapter. Due to the rotation generated by the tool spindle, a scanning roller passes through the cam disk ($d = 240$ mm), which is provided with a cross-sectional contour scaled by a factor of three. The radial change in position of the scanning roller viewed from the centre point is converted into a rotational movement by a claw connection and transmitted to the oscillating pole of the special boring bar. The oscillating pole ($l = 5,620$ mm, $d = 28$ mm)

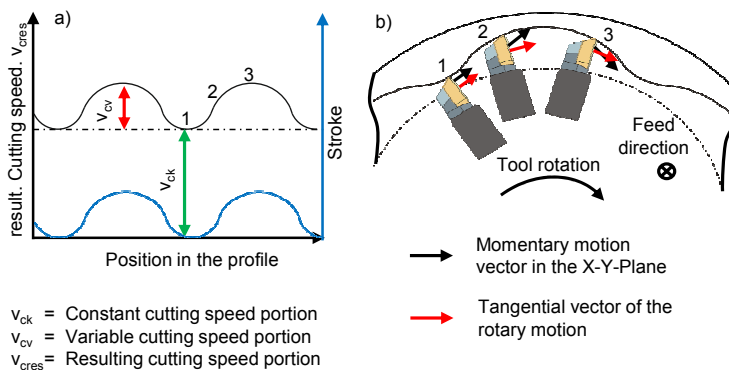
is connected to a positioning mechanism in the drill head. The drill head ($d = 46$ mm) contains an eccentric in the front part, which extends and retracts a slider equipped with an indexable cutting insert - depending on the contour of the cam disk.

2.2 Description of the cutting speed variation

Due to the stroke of the slider, the resulting cutting speed v_{res} changes continuously. On the one hand, this consists of the minimum cutting speed, the constant cutting speed v_{ck} . On the other hand, it consists of a variable cutting speed component v_{cv} , which results from the stroke. Figure 3(a) describes how the resulting cutting speed and the stroke behave as a function of the profile position. The cutting speed, on the left vertical axis, and the stroke, on the right vertical axis, are illustrated qualitatively. The figure shows that the stroke varies periodically and the minimum stroke is zero. The variable cutting speed component, like the stroke, has zero as its minimum value. The resulting cutting speed and the stroke behave qualitatively the same. Quantitatively, the resulting cutting speed is always increased by the constant cutting speed component.

The periodic motion of the stroke also affects the motion vector of the cutting edge. In conventional turning or drilling processes, the motion vector is almost tangential to the circular rotary motion. Due to the retraction and extension of the cutting edge, the motion vector is not tangential to the circular rotary motion of the drill head. Figure 3(b) shows the cutting edges at three different positions of the profile.

Figure 3 (a) Cutting speed v_c in relation to the stroke and (b) position in the profile (see online version for colours)



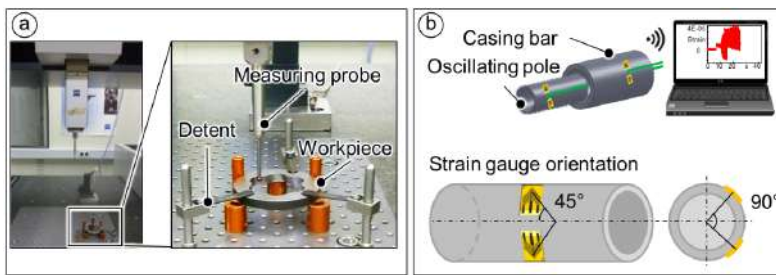
The momentary motion vector and the tangential vector of the rotary motion of the drill head are drawn on the cutting edge. The first position shows the cutting edge in a low point of the profile. The stroke is zero. At this point, the cutting edge is neither retracting nor extending. The cutting edge experiences the same situation at the maximum stroke, at the highest point of the profile. At these two points, the motion vector of the cutter has the same direction as the tangential vector of the rotary motion. The next position shows the cutting edge in the extension movement. Motion vector and tangential vector do not point in the same direction. The motion vector is directed 'outward'. The difference in direction results from the stroke by which the cutting edge moves away from the centre of the profile. The last position shows the cutting edge in the retracting

motion. The movement vector in this case points in the direction of the centre of the profile. The vector undergoes a change of direction due to the retraction movement. The difference between the tangential vector and the motion vector depends on the pitch of the profile flanks.

2.3 Overview of the used measurement technologies

The machined test specimens were sawed into slices approx. $t = 10$ mm thick. Before measuring, the specimens were positioned and clamped onto the table of the coordinate measuring machine as seen in Figure 4(a). The measuring cycle was force-regulated the measurement direction was the opposite of tool rotation. A total of 365 measuring points were recorded along the circumference. The contour profiles are output by spline interpolation of the measuring points. The measured contours were always oriented identically in relation to the target profile in order to be able to establish comparability. These contours were used to evaluate the manufactured profile depending on the test parameters and tool designs.

Figure 4 (a) Coordinate measuring machine with clamped profile sample and (b) structure of the measurement technology (see online version for colours)



To measure the torsional moment, strain gages were attached onto the casing bar and the oscillating pole (Figure 4(b)). The measurements and data transmission were realised with a NI-cDAQ-9191 WiFi chassi, a NI-9237 bridge module, a separate power supply and an antenna for wireless data transmission. These components were positioned inside the tool spindle to rotate during the process. Using a standard router and the measuring laptop a wireless network was set up. Via the network, it was possible to transmit live data while machining with rotating spindle.

2.4 Workpiece material and probe geometry

The materials used for the chamber boring experiments were two steel alloys (42CrMo4+QT/AISI4140, C60/AISI1060) and one aluminium alloy (AlMgSi0,5/EN AW-6060). The round bars had a diameter of $d = 80$ mm a length of $l = 250$ mm and were pre-drilled and honed with a bore diameter $D_B = 46$ mm and a tolerance range H7 [DIN EN ISO 286-1:2019-02]. The mechanical properties of the materials are displayed in Table 1.

Table 1 Mechanical properties of the test materials

<i>Material</i>	<i>AISI 4140</i>	<i>AISI 1060</i>	<i>EN AW-6060</i>
R_m in MPa	900–1100	>670	≥190
$R_{p0.2}$ in MPa	≥650	≥340	≥150
Hardness in HB	≤255	≤241	≥65
Density in kg/m ³	7.9	7.8	2.7
Heat treatment	Quenched and tempered	Normalised	Precipitation hardened

Source: DEW (2021), DELTA (2021) and Saerstahl (2021)

The aluminium alloy was used because lower forces occur while machining, so the load on the drive would be lesser and the risk of severe damage would be smaller. The AISI 1060 is a non alloy carbon steel for heavy duty fabricated parts due to combination of high tensile strength and good machinability it is used in many industry applications i.e., gearshift fork, gears or agricultural machinery attachments. The chromium molybdenum alloy steel AISI 4140 is a quenched and tempered steel known for its high strength with high toughness at the same time. Therefore, it is used for highly stressed components i.e., drill collars, axles, gear shafts or crankshafts (DEW, 2021; DELTA, 2021; Saerstahl, 2021).

3 Comparison of two slider kinematics

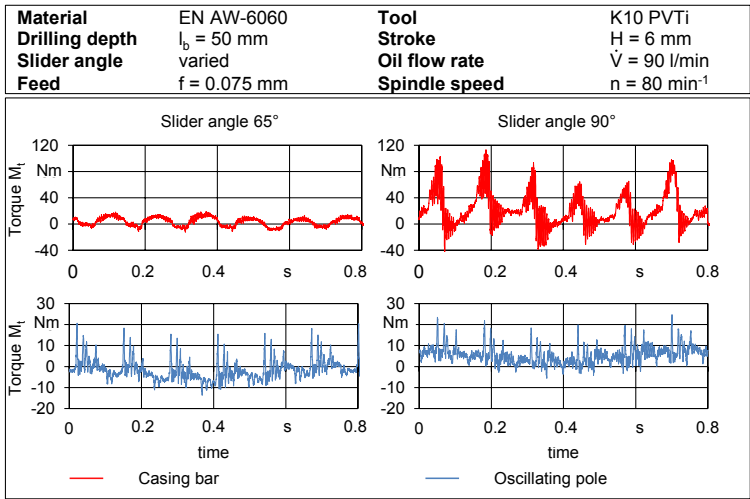
3.1 Influence of the slider angle

The first step was to analyse the influence of the slider on the AK-UR process. The torsional moments of the process are compared for identical cutting parameters in Figure 5 for the two slider variants. The increase and decrease (waveform) of moments outlined in the diagram occurs during the machining of a profile chamber. The section shown with the six high points results during one rotation of the drill head. The negative moments result from the torsion and the mass inertia of the casing bar and the oscillating pole. The comparison shows that the tool load increases significantly when using the 90°-slider. For the casing bar, there is a 216% increase in torsional moments on averaged over six chambers. The maximum unfiltered torsional moment of the casing bar, which is caused by the engagement of the 90°-slider, is $M_t = 112.3$ Nm, whereas only $M_t = 18.7$ Nm is measured for the 65°-slider. The maximum unfiltered torsional moment of the oscillating pole resulting from the usage of the 90°-slider is $M_t = 23.4$ Nm, compared to $M_t = 17.2$ Nm for the 65°-slider. For the 90°-slider, a higher base load is found, whereas the torsional moments fluctuate around the zero point.

The cause of this process can be seen Figure 6. For both slider variants, the passive force F_p , the feed force F_f and their resultant, which is labelled F_{pf} , are drawn as examples. It should be noted that the vector amounts in the drawing are identical, although the forces in the real process differ due to the different chip thickness and chip width resulting from the engagement condition. If the resultant F_{pf} is applied to the slider contact surfaces, taking into account their positioning (65° and 90°), it is noticeable that the tangential force F_t , which acts on the oscillating pole, is significantly higher for the 90°-slider. Since the tangential force F_t for the 90°-slider acts in the vertical direction, it

corresponds to the vertical tangential force $F_{t,v}$. For the 65°-slider, the tangential force must be split into a horizontal and a vertical component. This results in the higher load on the oscillating pole for the 90°-slider, since for the 65°-slider the normal force component F_n and the horizontal component of the tangential force F_t , are absorbed by the drill head and supported on the workpiece. The fluctuating value of the torsional moment of the oscillating pole is caused by the influence of the slide plate, including attachments with a weight of approx. $m = 3.1$ kg, on the AK-UR drive, since it is either guided on the guides or acts completely unguided on the oscillating pole, depending on its position. Due to the lower loads, this influence is more clearly reflected in the torsional measurements of the oscillating pole for the 65°-slider. In addition to the high torsional forces in the engagement, another reason for the failure of the 90°-slider in the steel materials is the abrupt start of the cut. For the 65°-slider, for a speed $n = 80 \text{ min}^{-1}$ and a feed rate of $f = 0.075 \text{ mm}$, the starting time or time until full engagement of the cutting edge is $t_{start,65} = 25.65 \text{ s}$. In contrast, the 90°-slider is completely engaged after $t_{start,90} = 8.71 \text{ s}$ at identical cutting parameters.

Figure 5 Influence of the slider angle on the torque M_t (see online version for colours)



The immense difference of the torsional moment at the casing bar is caused by a tilting of the cutting edge slider in the drill head for the 90°-slider. Theoretically, the chip section A is identical for both sliders, since the feed f and the cutting depth a_p are constant. However, tilting the 90°-slider results in a massive increase in the chip section and thus in an enormous increase in the cutting force F_c . The tilting of the 90°-slider could be verified in the machined aluminium EN AW-6060 workpieces, since indentations of the guide pads, which are mounted to the drill head, are visible in the bore surface of the guide bore. One possible reason for the tilting is that the slider starts rubbing in the incline profile of the bore wall. This could be identified by marks on the slider and by the smoothed area in the profile. As a result, machining of AISI 1060 or AISI 4140 is not feasible with the 90°-slider, as it leads to breakage of the insert or the slider fixture. As an example, Figure 7 shows a slider used in AISI 1060 and a used insert that was destroyed

during the process. In the left section a photo of the destroyed slider is shown. The increased forces led to a break of the insert seat. On the right is the broken out insert of the process photographed.

Figure 6 Comparison of the engagement conditions of the slider variants (see online version for colours)

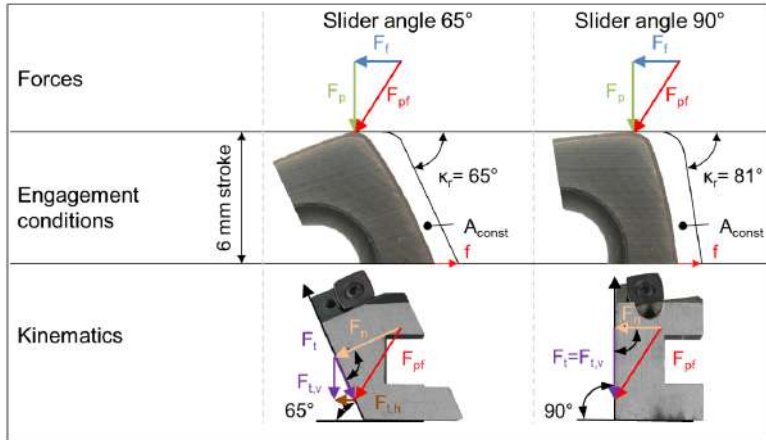




Figure 7 Broken slider with 90° slider angle during machining of AISI 1060 (see online version for colours)

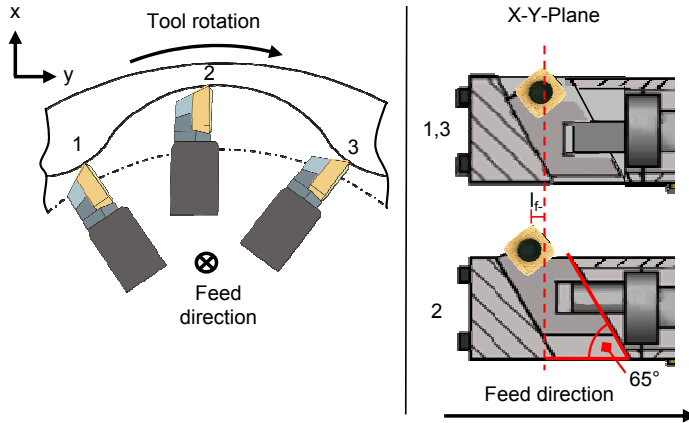
Material	AISI 1060	Tool	K10 PVTi
Drilling depth	varied	Stroke	H = 6 mm
Slider angle	90°	Oil flow rate	$\dot{V} = 90 \text{ l/min}$
Feed	varied	Spindle speed	varied

		
		Minor cutting edge
		Major cutting edge

3.2 Influence of the 65°-slider angle on the machined profile

The stroke influences on the cutting speed, as described in Section 2, and the direction and the position of the cutting edge in the feed direction. Figure 8(a) shows the cutting edge at the start, high point and end of a profile convexity. Figure 8(b) shows the movement of the cutting edge in the feed direction as it passes through the three points. Figure 8(b) shows that while the cutting edge moves along the profile, it is not positioned in the same X-Y plane at all times. Instead, during the extension movement, the cutting edge is moved against the feed direction until the maximum stroke is reached. The retract motion moves the cutting edge, in the feed direction, back to the original X-Y plane. For the consideration of the offset (l_f), a feed rate $f = 0$ was assumed. With a feed $f \neq 0$ positions 1 and 3, in Figure 8(b), would not be in the same plane.

Figure 8 Position change of the cutting edge in feed direction due to the stroke (see online version for colours)



The offset against the feed direction results from the design of the slider. In Figure 8(b) it is also illustrated that the movement of the slider is not orthogonal to the feed direction, but at an angle of 65° . The influence of this design is shown below using a fictitious example. The following assumptions are to apply to the example:

- | | |
|--------------------------------|---|
| • Profile with six convexities | • Profile pitch: 360° rotation of the profile after a drilling path $l_b = 500$ mm |
| • Feed $f = 0.06$ mm | • Spindle speed $n = 60$ min ⁻¹ |
| • Stroke $H = 6$ mm | • Slider angle $\theta = 65^\circ$ |

A drilling path of $l_b = 0.06$ mm is covered per revolution. When passing through one convexity, a drilling path of $l_b = 0.01$ mm is covered. With reference to Figure 8(b), the offset between points 1 and 3 in the feed direction would be $l_{f+} = 0.01$ mm. The offset l_{f-} can be calculated from the data using the following formula:

$$l_{f-} = \frac{H}{\tan 65^\circ} = \frac{6 \text{ mm}}{\tan 65^\circ} \approx 2.8 \text{ mm} \quad (1)$$

While the cutting edge moves from point 1 to point 2, a feed path in the feed direction of $l_{f+} = 0.005$ mm is covered by the drill head. This portion is less than 1% of the offset against the feed direction and is therefore neglected. For simplification, we assume that the starting and end points of a profile convexity are in the same X - Y plane and are passed in the same revolution. The resulting profile is shown in Figure 9.

The upper area in Figure 9(a) shows that the start and end points of the profile convexities are positioned in one X - Y plane with $Z = 0$. The highest points in the profile are on the X - Y plane with $Z = 2.8$ mm. The X - Z diagram illustrates the consequence of the offset against the feed direction. The profile produced in one rotation appears like a profile curve whose convexities are oriented at an angle of $\alpha = 65^\circ$ with respect to the X - Y plane. To machine a complete convexity in the one X - Y plane, the position of the cutting edge in point 1, 3 and 2 has to be in this plane. This state is achieved if the offset (l_{f-}) is covered by the feed, which takes numerous revolutions to complete. The number

of revolutions (R) and the time (t) required to cover this offset can be calculated. The equations used are as follows:

$$R = \frac{l_{f-}}{f} = \frac{2.8 \text{ mm}}{0.06 \text{ mm}} = 46.6\overline{6} \approx 47 \text{ with } n = 60 \text{ min}^{-1} \quad (2)$$

$$t = \frac{R}{n} = \frac{47}{60 \times 60 \text{ s}^{-1}} = 47 \text{ s} \quad (3)$$

$R = 47$ revolutions or $t = 47 \text{ s}$ are required to cover the offset with the assumed parameters. This means that a profile in the X - Y plane is produced in $R = 47$ revolutions. From the assumption that starting and end points of a profile convexity are part of the same X - Y plane, it follows that two points located in the same X - Y plane are machined in each subsequent revolution. The exception is the highest point of the convexity.

Figure 9 Machined profile in the X - Y and X - Z -plane (see online version for colours)

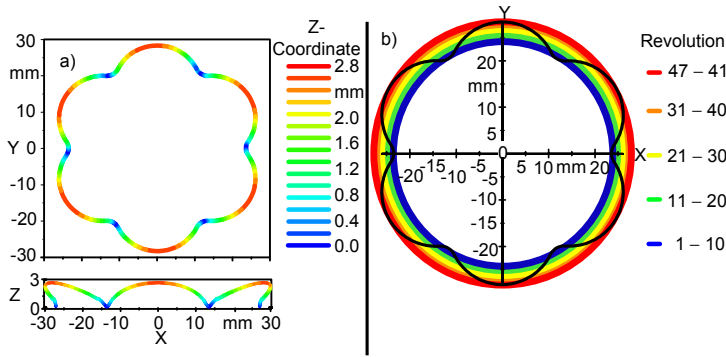
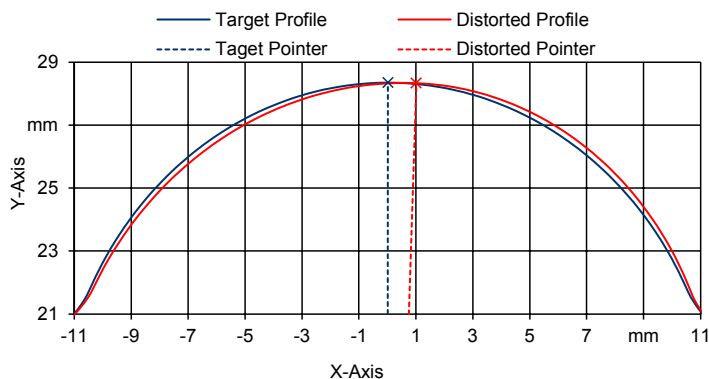


Figure 9(b) shows the profile in the X - Y plane and its structure. In a real process, the cutting edge is moved continuously by the feed. This means there are no individual points that are created, but sections of the profile. The relationship of the profile sections to the respective revolution in which they were manufactured is marked by coloured circles.

If a profile is manufactured without a pitch, the offset and the resulting cutting edge curve per revolution can be neglected. However, in this process the profile pitch per drilling path $l_b = 500 \text{ mm}$ is 360° . Due to the pitch follows, for a profile in the X - Y plane, that the starting and end point of a convexity are manufactured with a differently oriented cam disk compared to the high point. While the offset (l_{f-}) is being covered, the cam disk rotates in the drive which results in a distortion of the manufactured profile. The angle of rotation of the cam disk (ξ) can be determined as follows:

$$\xi = \frac{360^\circ}{l_b} \times l_{f-} = \frac{360^\circ}{500 \text{ mm}} \times 2.8 \text{ mm} = 2.0^\circ \quad (4)$$

The successive sections in the profile experience only a fraction of the total distortion. In this example the profile is machined in 47 revolutions, during which it is rotated by $\xi = 2.0$. Per revolution, the distortion is approx. $\xi_R \approx 0.04^\circ$. The impact of this distortion was calculated for one profile convexity in 78 points and is shown in Figure 10.

Figure 10 Distorted profile convexity in the X - Y -plane (see online version for colours)

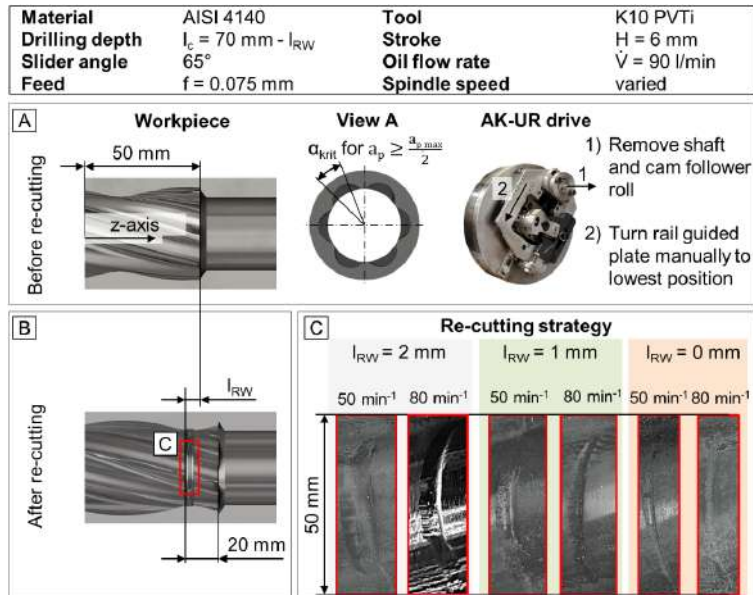
The distorted profile appears shifted in the direction of the positive X -axis. Start and end areas of the curves show significantly smaller deviations than, for example, the flanks of the profile. On the flank with a positive inclination, the distorted profile runs less steep than the target profile. The opposite effect can be observed on the other flank. The point of intersection of the two curves is located in the area around the high point of the profile. Due to the slider and the pitch the profile is distorted in such a way that the positive profile gradient decreases and the negative profile gradient increases. The profile flanks become flatter on one side and steeper on the other, in contrast to the target profile. Furthermore, the high point of the profile shifts towards the steeper flank. The two pointers in the diagram illustrate the distortion in X -direction. The two pointers start in the centre of the profile at $X = 0$ mm and $Y = 0$ mm which is not visible in the diagram. The blue target pointer shows the position of the highest point of the desired profile; the red distorted pointer shows the same point after the distortion was added. The distortion in X -direction of this two points amounts to approx. 1 mm.

4 Re-cutting strategy

As explained in the prior part, internal contouring is of particular interest for workpieces of great length. The wear tests performed with the AK-UR system revealed two main reasons for insert breakage. One of the main reasons is the large number of load changes combined with large forces due to insufficient chip evacuation. In addition, adhesive wear can be detected on the protective chamfer of the carbide insert after drilling lengths of $l = 800$ mm. Likewise, the large number of load changes at this bore length favours sudden fatigue fractures. With a feed of $f = 0.075$ mm, six profile chambers, two load changes per profile convexity and a drilling length of $l_b = 800$ mm, this results in 128,000 load changes affecting on the carbide insert. As a consequence, changing the insert is the only way to achieve the desired bore length. This procedure poses a high technical challenge, since the positioning of the workpiece as well as the orientation of the drive in relation to the profile contour cannot be changed. A slight change in the workpiece

position or orientation causes a twisted position of the already created contour, so that no aligned recut is possible in the previously created profile. That would lead to an immediate destruction of the insert, the slider as well as the drill head and the workpiece. The procedure for performing the recut in the profile is explained below and outlined in Figure 11.

Figure 11 Visualisation of the developed re-cutting strategy (see online version for colours)

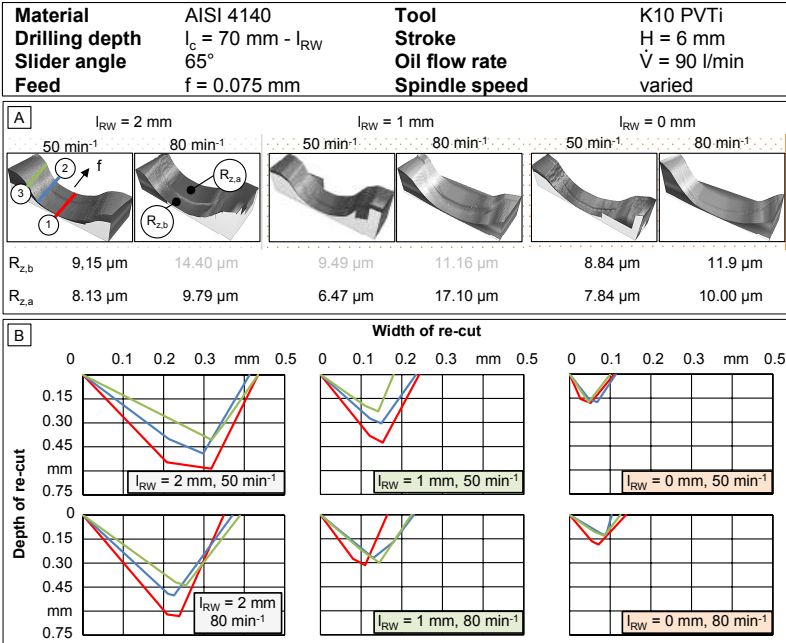


The first thing is to stop the process and drain the bore oil from the bore. Then remove the shaft and the cam follower roll in the slide drive and turn the rail guided plate manually to the lowest position in the profile. This pushes the slide and the insert beneath the already machined profile contour and the drill head can be moved out of the workpiece into a chuck with a maintenance cover. With this chuck the drill head can be accessed while the workpiece is still clamped. The insert is changed and the drill head is moved back into the workpiece. The already internally contoured drilling length must be reduced by the reset length l_{RW} . In experimental test series, the influence of different reset lengths on the recut was investigated and is shown in Figure 12.

Figure 12 shows the results of the different re-cutting strategies for two spindle speeds. Area A shows the digitised re-cuts and the three measuring positions for determining the width and depth of the re-cut. In addition, the positions for determining the average roughness depth $R_{z,b}$ before and $R_{z,a}$ after the recut are noted. The analysis shows that the roughness depth R_z is always lower after the re-cut with a new cutting insert due to adhesive wear. The R_z values marked in grey are excluded because of the insufficient digitised area. Regardless of the chosen strategy, the cut is always performed in the correct profile pitch. For each strategy, the greatest depth is identifiable at the high point of the profile (stroke = maximum) (see area B, course of the red curves). No trend is discernible as a function of the spindle speed. Furthermore, it can be seen that with a

lower l_{RW} value, the incision depth and thus the contour error is reduced. If l_{RW} is reduced from 2 mm to 0 mm, an average reduction of the incision depth by approx. 70% is possible.

Figure 12 Influence of re-cutting strategy on the profile contour (see online version for colours)

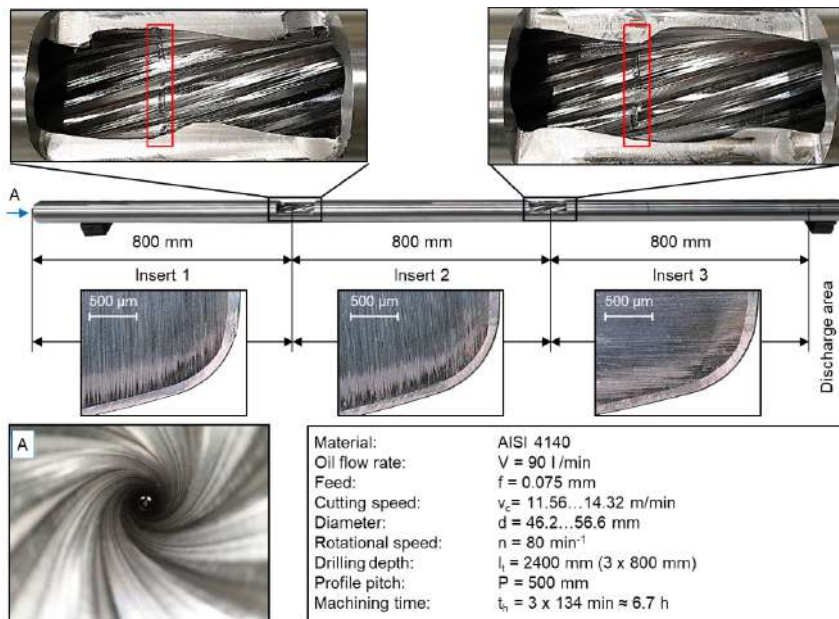


5 Outlook and conclusion

The enlarged image section in Figure 13 show the generated internal profiling, which was produced in a total process time of $t = 6.7 \text{ h}$. The total drilling depth is $l_b = 2400 \text{ mm}$ and was produced in three process segments ($3 \times 800 \text{ mm}$). The red marks indicate the recut areas, which are performed for $l_{RW} = 2 \text{ mm}$. Furthermore, the detailed images of the inserts used are shown after the respective section. The marked run-out area is used for better guidance of the drill head and is not machined. The pre bred run-out area prevents the drill head from entering the drill bushing and causing axial displacement, which would result in failure of the insert.

Finally, a recutting strategy in the bore profile has been developed, in which the process is stopped after $l_b = 800 \text{ mm}$ of drilling depth and the insert can be changed. Subsequently, the process is continued in the stopping point of the workpiece. The maximum bore length thus achieved is $l_b = 2400 \text{ mm}$ and has been produced in a process time of $t = 6.7 \text{ h}$. Since adhesion wear has been identified as the cause of insert weakening, the variation of the insert coating represents a subject area with great potential for future research. In addition, the production of an adjusted cam disk for the mechanically coupled drive concept is conceivable, so that the analysed contour inaccuracies can be reduced.

Figure 13 Chamber bored workpiece with two tool changes after $l_b = 800$ mm and $l_b = 1600$ mm drilling depth (see online version for colours)



6 Conclusion

- A novel as well as unique method for the production of internally profiled workpieces with small internal diameters is presented.
- The application in highly demanding materials has been made possible by an adapted tool/slider geometry.
- The resulting profile distortion is analytically determined and calculated.
- Due to the developed recutting strategy the cutting edge can be changed mid process.
 - With this strategy the maximal length of the bore is limited by the machine, not the tool life.
- The technological gap regarding the machining of a metallic base profile was narrowed.
 - This process enables the production of more powerful and more compact MUD drives.
 - The efficiency of directional drilling systems for the exploration of oil and gas deposits can be increased.

References

- Baker Hughes (2020) *Navi-Drill Motor Handbook* [online], 15th Edition Rev A, <https://www.bakerhughes.com/sites/bakerhughes/files/2020-11/Baker-Hughes-Navi-Drill-motor-handbook-15th-edition-2020.PDF> (Accessed 20 July, 2021).
- Biermann, D., Bleicher, F., Heisel, U., Klocke, F., Möhring, C. and Shih, A. (2018) ‘Deep hole drilling’, *CIRP Annals*, Vol. 67, No. 2, pp.673–694.
- Bottos, R.D. and Underwood, L.D. (2003) *Method of Making an Internally Profiled Stator Tube*, United States Patent 6568076B2.
- Buse, B., Bergmann, K. and Fuß, H. (1994) ‘Flexible internal machining with computer-controlled drilling tools (in German)’, in Weinert, K. (Eds.): *Spanende Fertigung 1*, Vulkan-Verlag, Essen.
- DELTA-TRADING GmbH Metallhandel (2021) AlMgSi0,5: EN AW-6060 -3.3206 – AlMgSi0,5 - Material datasheet. http://www.delta-trading.de/fileadmin/edit/datenbl%C3%A4tter/EN_AW-6060_-_3.3206_-_AlMgSi0_5_-_Werkstoffdatenblatt.pdf (Accessed 17 September, 2021).
- Denkena, B., Grove, T., Eggemann, K., Wissel, R. and Pape, O. (2016) ‘Tool development for stator production (in German)’, *mm Maschinenmarkt*, Ausgabe 8, [online] ID:44125971, <https://www.maschinenmarkt.vogel.de/werkzeugentwicklung-fuer-die-statorherstellung-a-545173/> (Accessed 20 July, 2021).
- Deutsches Institut für Normung e. V. (2019) *EN ISO 286-1:2019-02: Geometrical Product Specifications (GPS) – ISO Code System for Tolerances on Linear Sizes - Part 1: Basis of Tolerances, Deviations and Fits*, Berlin, DIN.
- DEW – Deutsche Edelstahlwerke Specialty Steel GmbH & Co. KG (2021) *Material Datasheet 42CrMo4/AISI4140 (in German)*, https://www.dew-stahl.com/fileadmin/files/dew-stahl.com/documents/Publikationen/Werkstoffdatenblaetter/Baustahl/1.7225_1.7227_de.pdf (Accessed 17 September, 2021).
- Fuß, M., Abrahams, H., Buse, B. and Biermann, D. (2016) ‘Production of Deep Bore Holes with Non-Circular Profiles’, *Journal of Advanced Materials Research*, Vol. 25, pp.197–204.
- Heisel, U. and Utz, T. (1989) ‘Chambering by milling (in German)’, *Dima 43*, Vol. 6, pp.16–23, <http://dx.doi.org/10.18419/opus-4240>
- Malcore, E. (2012) ‘Reservoir drives choice of RSS vs. mud motors.’ *Drilling Contractor*, March–April [online] <https://www.drillingcontractor.org/reservoir-drives-choice-of-rss-vs-mud-motors-14018> (Accessed 20 July, 2021).
- Maurer, W. (2000) *Advanced Geothermal Turbodrill*. [online] Final Report DE-FGO7-98ID 13680, Maurer Engineering, Inc. for U.S. Department of Energy. <https://www.osti.gov/servlets/purl/765115> (Accessed 20 July, 2021).
- Saarstahl, A.G. (2021) *Material Datasheet C60R/AISI1060 (Cm60) (in German)*, <https://www.saarstahl.com/sag/downloads/download/11018> (Accessed 17 September, 2021).